npj | climate and atmospheric science

www.nature.com/npjclimatsci

ARTICLE OPEN

Check for updates

Aerosol processes perturb cloud trends over Bay of Bengal: observational evidence

Sunny Kant[1], Chandan Sarangi[1,2,3]✉ and Eric M. Wilcox[4]

Although, the aerosol-cloud interactions and its impact on daily to seasonal radiation/temperature has been well observed over South Asia in last two decade, the role of aerosol-cloud interactions on cloud occurrence trends (and surface temperature) is yet not evident. Here, evidence of aerosol-induced control on cloud occurrence trends over the Northern Bay of Bengal (NBOB) during the monsoon onset period is presented. In last 15 years, increased aerosol emissions over North India have led to an increase in aerosol loading at an elevated altitude of 1–3 km over the NBOB outflow region in monsoon onset period. This elevated aerosol loading induces increases the air temperature at 1–2 km altitude and stabilizes the lower troposphere over the region in recent years. The enhanced atmospheric stability in the region caused low-level cloud occurrences (below 3 km) to increase in recent years by ~20%, potentially contributing to the observed non-intuitive cooling trends in sea surface temperatures. These aerosol-cloud-climate observations emphasize the crucial need for improved aerosol representations in coupled ocean-atmosphere models for accurate predictions of climate change over South Asia.

npj Climate and Atmospheric Science (2023)6:132 ; https://doi.org/10.1038/s41612-023-00443-x

INTRODUCTION

Aerosol-Cloud-Radiation-Climate interactions are a significant source of uncertainty in climate forcing[1–4]. First, aerosols can serve as cloud condensation nuclei (CCN) for the formation of cloud droplets and consequently influence cloud physical properties by increasing the cloud lifetime, and albedo causing a negative radiative forcing[1,2]. Second, the presence of anthropogenic absorbing aerosol also tends to induce atmospheric warming and decrease liquid cloud water path, and cloud cover due to the semi-direct effect (SDE)[5]. Many previous studies using satellite observations and modeling report that cloudiness of low-level clouds decreases within a polluted boundary layer in presence of absorbing aerosols leading to a positive radiative forcing[6–9]. For instance, the influence of aerosol heating on marine stratocumulus clouds over the southeast Atlantic Ocean can cause a SDE of 15 Wm^{-2} using the large-eddy model[10]. Nonetheless, the response of low-level clouds to the SDE depends upon the vertical heating of the aerosol profile[6,10]. The presence of absorbing aerosols above the low-level cloud layer results in a decrease in cloud-top entrainment and consequently low-level cloudiness increases due to a thickening that induces a negative SDE forcing[9–13]. Such a negative radiative forcing due to cloud adjustments to SDE can largely offset the direct positive forcing from the presence of absorbing aerosol[5,6,10,14,15].

Many sensitivity studies using the climate model found that increasing absorbing aerosols leads to enhanced global mean low-level clouds, but a decrease in mid, and high-level clouds[13,16,17]. Nevertheless, observational studies with evidence of SDE-induced enhancement in low-level clouds is rare. For example, Norris[18] using the Indian Ocean Experiment (INDOEX) observation reported only a marginally increasing trend of low-level clouds in the presence of increased absorbing aerosol loading over the northern Indian Ocean. That study argued that an increase in the trend of SST-enhanced evaporation, and hence surface buoyancy, compensates for any aerosol-induced warming and drying of the boundary layer. In contrast, an examination of multiple observations such as surface observations, International Satellite Cloud Climatology Project, and Indian National Satellite System concluded that the trend of nonoverlapped cumulus clouds is decreasing over the Indian marine regions consistent with SST warming and boundary layer stratification[19]. A Large-eddy experiment of boundary layer trade cumulus clouds during the Indian Ocean Experiments (INDOEX) campaign led to the conclusion that incoming solar radiation absorption by anthropogenic absorbing aerosols decreases boundary layer mixing, and in-cloud relative humidity, in turn causing a decreasing trend of low-level cloud cover by 25–40%[5]. Recent studies have also demonstrated the signatures of aerosol microphysical effect on low-level boundary layer clouds over IGP and BOB[20,21]. However, the impact of aerosol processes on the marine cloud trends around South Asia is not clear and robust in our understanding. A reconstruction of historical aerosols in a general circulation model over the outflow region of the US during the 1970 to 1990 period was performed and concluded that the increase in the aerosol loading over the period enhanced the cloud cover[22]. This suggests that pollution outflow regions could be the opportunistic natural laboratories for observing potential evidence of aerosol-cloud-temperature climatic associations.

The North Indian sub-continent, especially the Indo-Gangetic Plain (IGP), is one of the major hotspot regions for global pollution due to higher emissions of natural, and anthropogenic aerosols[23]. During the pre-monsoon months, westerly winds transport anthropogenic and dust aerosols from the North Indian region to the Northern Bay of Bengal (NBOB). There has been a ~3–6% per year increase in aerosol loading over the Bay of Bengal (BOB) region during the pre-monsoon months[24]. Evidence from the COVID-19 pandemic lockdown period suggests that the outflow of continental (anthropogenic) aerosol contributes to ~20–30% of

[1]Department of Civil Engineering, Indian Institute of Technology Madras, Chennai, India. [2]Center for Atmospheric and Climate Sciences, Indian Institute of Technology Madras, Chennai, India. [3]Geophysical Flows Lab, Indian Institute of Technology Madras, Chennai, India. [4]Division of Atmospheric Sciences, Desert Research Institute, Reno, NV, USA. ✉email: chandansarangi@civil.iitm.ac.in

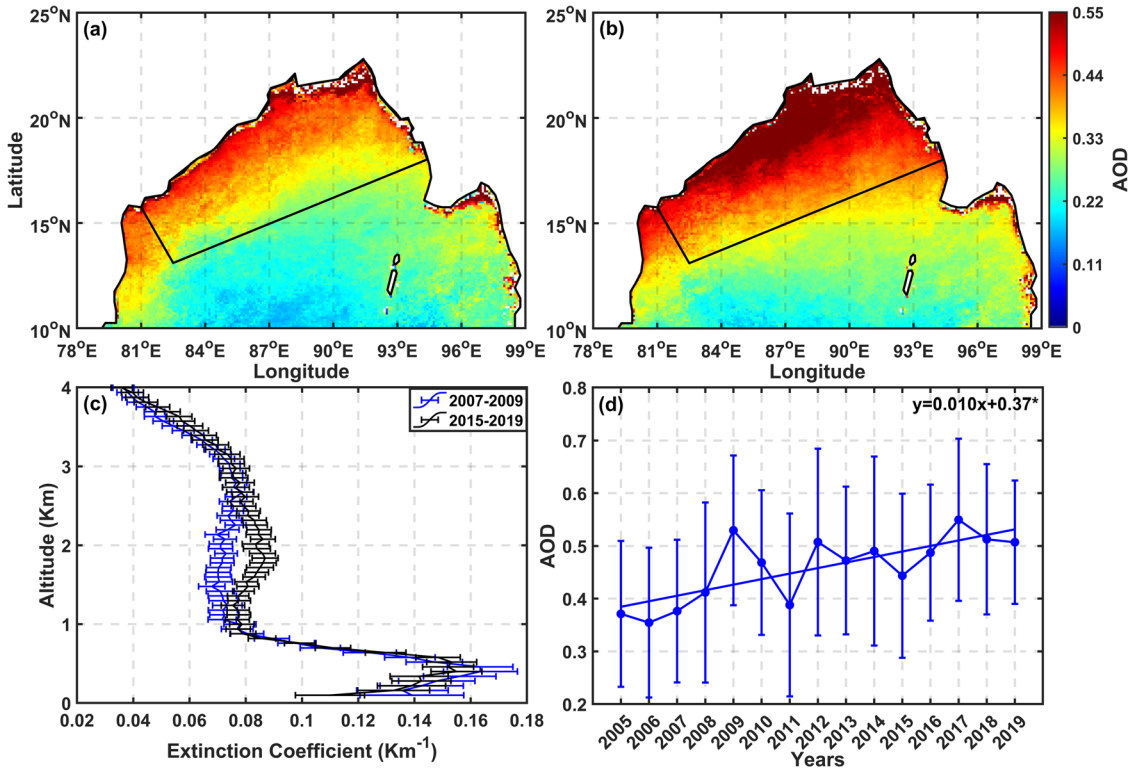

Fig. 1 Composite analysis and trends in aerosol loading over the NBOB. The spatial distribution of median AOD from MODIS/Aqua during the March to May (MAM) for the period of **a** 2005–2009 and **b** 2015–2019. **c** The vertical of extinction coefficient over the NBOB region for the period of 2007–2009 and 2015–2019. **d** The yearly trend in variation of AOD over the NBOB (black box). Standard error values are used for plotting the error bars and '*' symbol indicates the trend is statistical significance at a 95% confidence level.

the aerosol radiative forcing over NBOB[23] and can also affect the sea surface temperature (SST) values[25]. A study of satellite-based vertical profile of aerosol during the pre-monsoon months over the BOB found that dust from inland areas also contributes to 22% of the total extinction of aerosol[26]. Many previous studies have shown significant aerosol radiative and microphysical effects over the NBOB where continental aerosols flow out over the ocean[23,27]. For example, an aerosol-mediated atmospheric heating rate ~0.5 K day^{-1} is observed during the pre-monsoon months over north-eastern BOB due to the impact of anthropogenic aerosols, which influences the prevailing regional circulation[28]. The above points motivate us to analyze aerosol and cloud cover trends over NBOB (the outflow region of IGP) in recent decades. Further, it also instigates the question about can the aerosol-induced cloud changes (if any) affect the surface temperature/sea surface temperatures in the region under the widespread sea surface temperature rise in recent decades.

Here, we systematically examine long-term satellite data and illustrate robust trends in aerosol-induced low-level cloud cover enhancement over the NBOB region during the pre-monsoon (i.e., March-May) months, which in turn affects the SST trends.

RESULTS

Elevated Aerosol layers in outflow region of BOB

Fig. 1a, b show the spatial distribution of median aerosol optical depth (AOD) at 0.1° × 0.1° resolution during the monsoon onset months (MAM) for two 5-year periods representing a prior decade (i.e., 2005–2009), and a recent decade (i.e., 2015–2019). AOD is found to be higher in recent years (median value ~0.47) as compared to the past (~0.37), with an increase of ~27% over the NBOB (Fig. 1a, b) near the Indian coast of Bay of Bengal. In the composite of the earlier years, only a few grids with AOD values above 0.5 are found (Fig. 1a). The number of coastal grids with AOD > 0.5 increased distinctly and over a substantial area in recent years (Fig. 1b). The climatological median extinction coefficient profile observed by CALIPSO follows a parabolic shape variability w.r.t altitude with peak values at ~1–3 km altitude in both the present years than in the past years. More interestingly, the differences in CALIPSO observed extinction coefficient profiles between the two time periods show that the increase is mainly in an elevated layer between ~1 and 3 km above sea level. The elevated layers over the Indian outflow regions over the Bay of Bengal coast can be explained by the fact that aerosols rise to higher altitudes as they mix vertically through a deep boundary layer due to turbulence over the continent and then are transported horizontally over the ocean as they advect downwind[29–31]. The percentage of increase in the AOD composite (calculated between altitude of ~1–3 Km) of the recent years compared to that of the past years is ~30% (Fig. 1c and Supplementary Fig. 1a). The absorbing aerosol and polluted dust are increasing at the rates of 6.4×10^{-4} km^{-1} year^{-1}, and 4.4×10^{-4} km^{-1} year^{-1} respectively, while dust is decreasing at a rate of 7.2×10^{-4} km^{-1} year^{-1} between the elevated layer of 1–3 km over the NBOB (Supplementary Fig. 2). In these elevated layers during the pre-monsoon months, the aerosol is largely a combination of anthropogenic aerosols and polluted dust[2,3,32,33]. The chemical characterization of the aerosol study reported that percentages of mineral dust, black carbon, and particulate organic matter contribution over the NBOB region during the pre-monsoon were 25.93, 3.03, and 10.7%, respectively[34,35].

The seasonal median AOD is observed to have gradually increased from 2005 to 2019 over the NBOB region (Fig. 1d), apart from 2009 (Supplementary Fig. 2a), which was an abnormally dusty pre-monsoon year[32]. Specifically, the AOD is found to be increasing at a rate of 0.01 year^{-1} from 2005 till 2019 (Fig. 1d) and

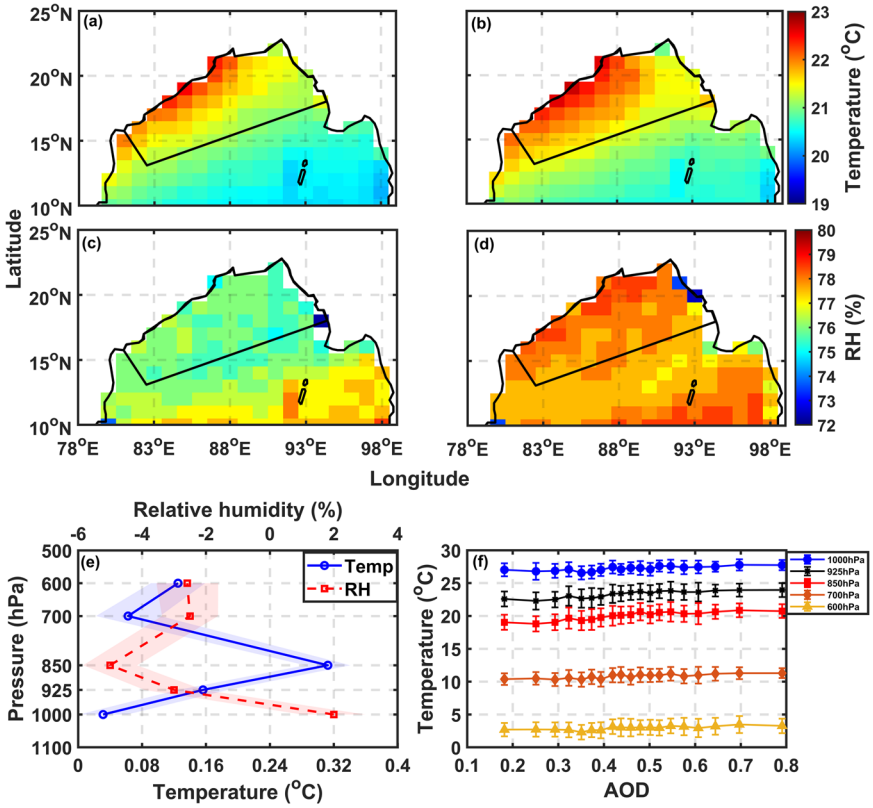

Fig. 2 Composite analysis of lower atmospheric stability and moistening over the NBOB. The spatial distribution of composite median temperature at ~900 hPa (**a**, **b**), and RH at 1000 hPa (**c**, **d**) from AIRS during March to May (MAM). The left column is composite median for the period of 2005–2009 (**a**, **c**) and the right column is same for 2015–2019 (**b**, **d**), respectively. **e** The difference between recent and past years of the temperature and RH vertical profiles. **f** The association of median temperature (at different levels) and columnar AOD over the NBOB (black box) region. Standard deviation values are used for plotting the bounded line and error bars.

9.6×10^{-4} km^{-1} year^{-1} at the elevated layer between ~1 and 3 km from 2007 to 2019 (Supplementary Fig. 3). The trend of AOD and extinction coefficient are statistical significance at a 95% significance level. This increasing trend in elevated aerosol loading over NBOB during the pre-monsoon months is mostly due to an enhancement in anthropogenic emissions over the Indian land mass in recent decades, which are transported via prevalent westerly winds, and deeper boundary layer heights from Indian landmass to the NBOB region[3,36–38]. Consistent with this, Thomas et al.[23] found that a reduction of aerosol loading over IGP by ~10–25% during the COVID lockdowns led to a 20–30% decrease in aerosol loading in the outflow region over the NBOB.

Thermodynamics of the lower atmospheric stability and moistening

Next, profiles of the AIRS observed atmospheric temperature and relative humidity (RH) averaged over NBOB for past period of years and recent period of years is compared to identify the signatures of enhanced radiative forcing of the aerosols on the regional thermodynamics (Fig. 2). Consistent with the AOD enhancement, the temperature (median of 925 and 850hPa), and RH (at 1000 hPa) of this layer has increased in the recent period (21.85 °C, and 78%) compared to previous period (21.56 °C, and 76%) over the NBOB region (Fig. 2a, b). Moreover, the spatial pattern of the enhancement is similar to that of the AOD (Fig. 1a, b). Positive differences between the recent period and past period are found for atmospheric temperature (0.29 ± 0.15 °C at 925 and 850 hPa), and RH (2 ± 0.60% at 1000 hPa) over the NBOB region (Fig. 2a–d). The percentage changes in temperature and RH from the past period to the recent period are 1.35%, and 2.63% respectively.

The vertical profiles of the change of both temperature and AOD from the prior decade to the recent decade show that both have increased predominantly in the same elevated layer of ~1–3 Km (Fig. 2e). In contrast, RH shows a positive change at the surface (2%) and a negative change in (as much as −4%) above the surface to 700 hPa. The profiles of the change in temperature are opposite with the temperature change lowest at the surface and greatest at 850 hPa, while the change in RH is greatest at the surface and lowest at 850 hPa. The specific humidity (SH) profile rises throughout the column over the NBOB region. The positive change in SH is highest at 600hPa and lowest at the surface (Supplementary Fig. 4). The absorbing aerosol heating increases the temperature at the lower troposphere, causing the saturation vapor pressure to rise as specific humidity increases, resulting in a decrease in relative humidity for the same amount of atmospheric water vapor.

To link these thermodynamic changes with AOD over the NBOB, we examine the AIRS temperature at different altitudes as a function of AOD (Fig. 2f). The air temperature increases with increasing AOD at ~1–2 km i.e., 925 and 850 hPa where the AOD enhancement is highest. However, there is no significant dependence of temperature on AOD at other pressure levels either above 700 hPa or at surface level. The standard deviation of the temperature of each bin is attributed to intra-seasonal variation. The values of AOD are sorted in ascending order and divided into bins of 5 percentiles. As such, the values of lower tropospheric stability (LTS), expressed as the difference between temperature at 700 and 925 hPa, is larger during high AOD loading (for instance LTS ~ 12.63 °C for AOD ~ 0.7) compared to the same for AOD ~ 0.2 (LTS ~ 12.20 °C). The difference between temperature of 700 hPa and the surface, 700 and 925 hPa, 700 and

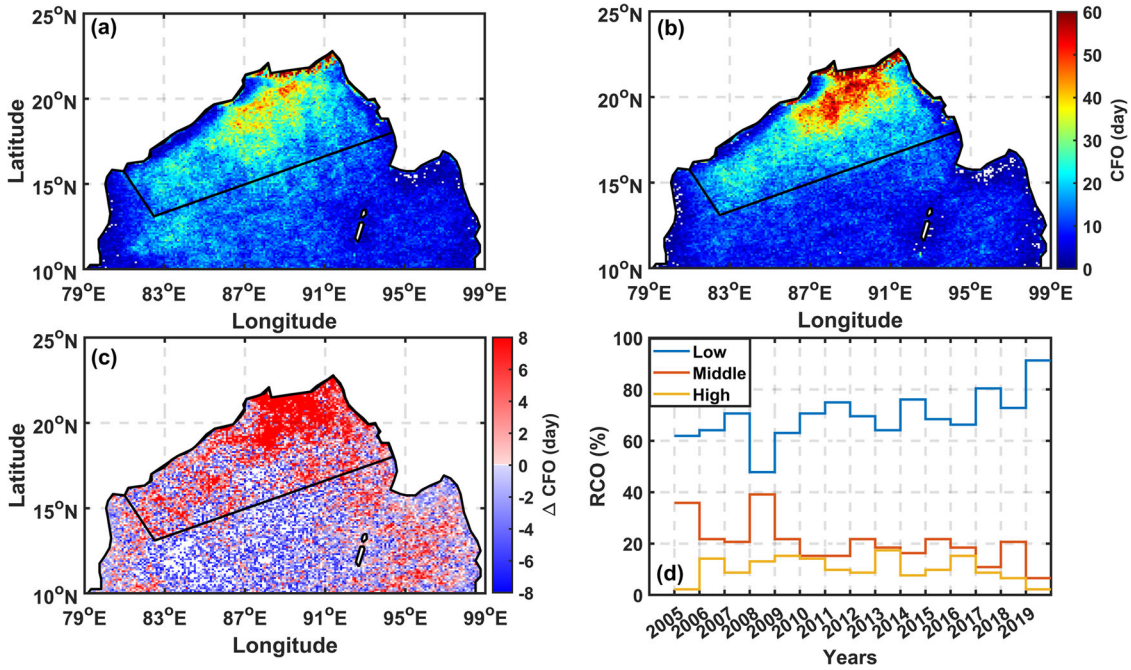

Fig. 3 Composite analysis and trends in cloud occurrences over the NBOB. The spatial distribution of median cloud fraction occurrences (CFO in day) during March to May (MAM) for the period of **a** 2005–2009 and **b** 2015–2019. **c** The difference in CFO over the region between the two composites: recent and past years. **d** Relative cloud occurrence (RCO) of low, middle and high levels of clouds over the NBOB (black box) region.

850 hPa is 16.35, 12.50, and 9.25 °C respectively for the period of 2005–2019. Thus, the large enhancement in lower tropospheric stability as aerosol forcing increases due to semi-direct effect is evident. Enhanced LTS can hinder vertical mixing and causes moisture trapping near the ocean surface[39], which explains our observations in Fig. 2c, d.

Further, the trend in the temperature (at 925, and 850 hPa), and RH (at 1000 hPa) over the NBOB region for the period of 2005–2019 has been analyzed (Supplementary Fig. 1b). More exactly, the trend of AOD is increased by 9.6×10^{-4} Km^{-1} $year^{-1}$ at the elevated layer of ~1–3Km from 2007 to 2019 over the NBOB. The temperature (925 and 850 hPa), and RH (1000 hPa) are observed to be increasing at the rate of 0.04 ± 0.42 °C $year^{-1}$, and $0.19 \pm 1.42\%$ $year^{-1}$ over the NBOB from 2005 to 2019. The increasing trend reveals that there has been a decrease in the turbulent flux in the mixed layer upward from the surface as the AOD has increased. The reduction in the turbulent heat flux has resulted in the surface mixed layer become warmer and thinner as aerosol radiative heating has increased in the elevated layer of ~1–3 Km. The decrease in the turbulent kinetic energy of boundary layer reduces the air entrainment across the inversion of temperature at the boundary layer top, which leads to larger RH in the surface mixed layer. As a consequence, cloud develops in a thicker saturated layer, and consequently, may penetrate above the top of surface mixed layer (inversion layer), since larger RH provides extra buoyancy to clouds[12]. In agreement, our result suggested that RH at surface (1000 hPa) is higher in the recent period of years as compared to the past years over the NBOB region (Fig. 2c, d).

Changing trends in cloud cover and SST over NBOB

Figure 3a, b shows the spatial distribution of cloud fraction occurrences (CFO) for low-level clouds (cloud top below 680hPa) at a spatial resolution of $0.1° \times 0.1°$ during the pre-monsoon months (MAM) during two time periods of prior years (i.e., 2005–2009), and recent years (i.e., 2015–2019). CFO is calculated for each grid as the percentage of days during MAM when cloud fraction was > 0.1. CFO is found to be higher in the recent years (26.89 days) as compared to the past years (22.66 days), with an increase of ~19% over the NBOB near the Indian coast of BOB (Fig. 3a, b). Note that the spatial pattern of change in CFO in the study domain is similar to that seen in case of AOD, i.e., the coastal region/grids show a distinct and substantial increase in CFO in the recent years (Fig. 3a, b). Specifically, the enhancement in the corresponding CFO is ~18–20% (Fig. 3c) which is of same order of magnitude to the aerosol loading enhancement (~20–30%).

Further, the trends in relative cloud occurrences for all the three different types of clouds [low-level (CTP > 680 hPa & COD < 100), mid-level (CTP = 440–680 hPa & COD < 100) and high-level (CTP < 440 hPa & COD < 100)] is analyzed to understand the overall changes in cloud climatology over the region. Relative cloud occurrence (RCO) over each grid of the domain and for each MAM season $year^{-1}$ is calculated i.e., CFO of that cloud type normalized by the total CFO (all cloud types) over each grid. RCO suggests that middle and high-level cloud occurrence decreased, and the occurrence of low-level clouds increased (Fig. 3d) as the extinction coefficient of the AOD trend has increased from 2005 to 2019 (Fig. 1d). Quantitatively, the RCO shows a clear increase in the low-level clouds in the recent period (75%) as compared to the prior years (61%). In comparison, there has been a decrease in the middle, and high-level clouds between the recent years and the prior years (−15 % and −8% respectively) over the NBOB region (Fig. 3d). Similar trends in median values of cloud fraction for low, middle and high cloud composites is also seen (Supplementary Fig. 6) clarifying that the observed trends in cloud occurrence is not a result of sampling changes across the years. Supplementary Figure 5a–c shows the probability distribution functions (pdf) of CDNC (cloud droplet number concentration), CWP (cloud water path), and cloud susceptibility (as per Eq. 2) for both the prior period and the recent period over the NBOB region. The mode values of pdfs for CDNC (15 cm^{-3}), CWP (26 gm^{-2}), and cloud susceptibility (0.3) are found to increase slightly during the present year composite compared to the CDNC (8 cm^{-3}), CWP (22 gm^{-2}) and cloud susceptibility (0.26) in the past years

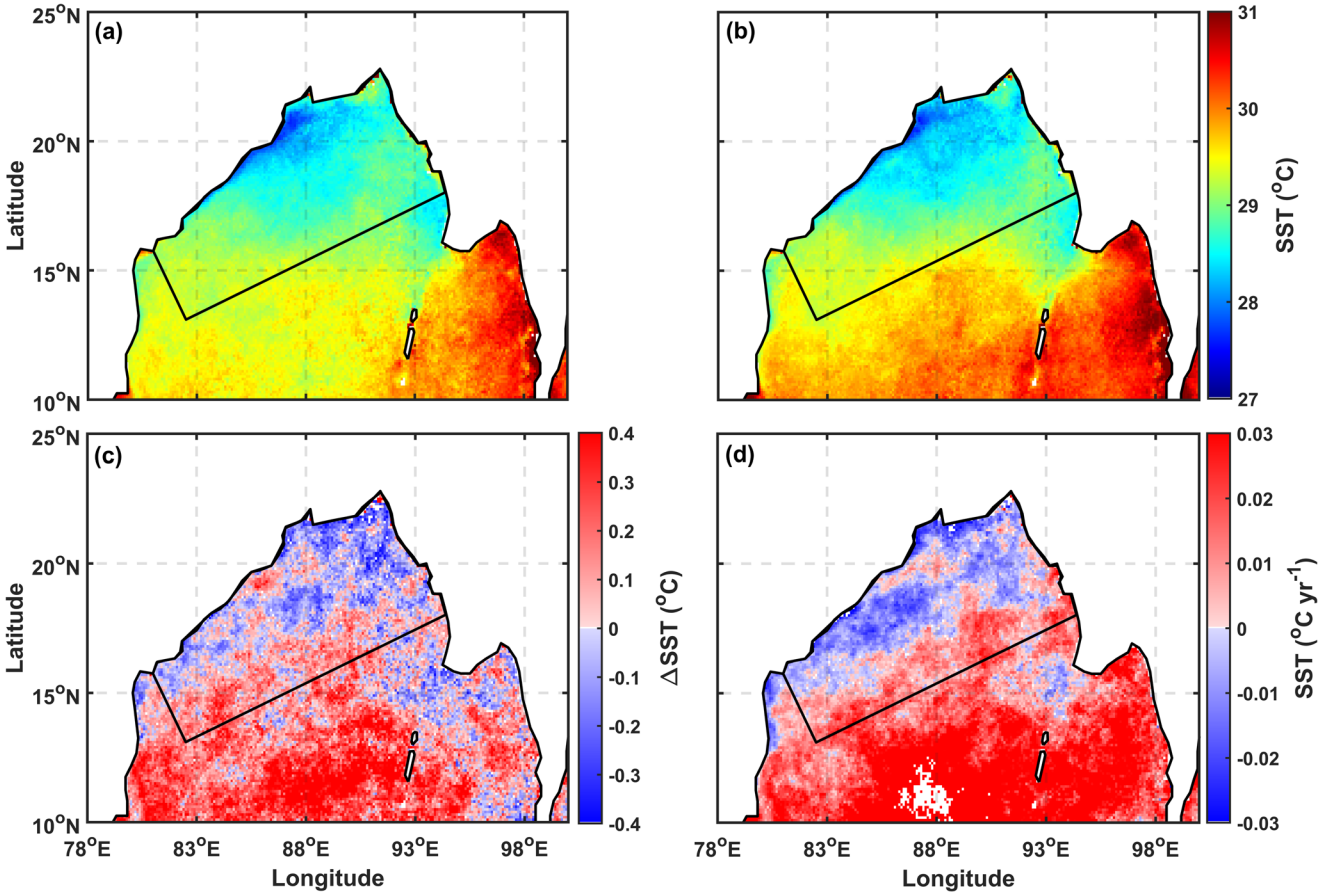

Fig. 4 Composite analysis and trends in Sean surface temperature over the NBOB. The spatial distribution of median sea surface temperature (SST) during March to May (MAM) for the period of **a** 2005–2009 and **b** 2015–2019. **c** The difference in composite median SST values between current (2015–2019) and past (2005–2009) years. **d** SST yearly trend from 2005 to 2019.

(Supplementary Fig. 5a–c). However, the change in CDNC values is not substantial, as previous modeling studies have shown than CDNC values need to enhance by orders of 5–10 to see substantial aerosol microphysical effect on small clouds[38,40,41]. Also, no change in drizzle rainfall over NBOB region was seen from TRMM satellite observations (Supplementary Fig. 9c). These points suggest that although some signals of aerosol microphysical perturbations are seen, the magnitude of impact was not consequential. Hence, the observed aerosol-induced cloud trend changes over NBOB are dominated by aerosol semi-direct effect.

Additionally, Fig. 4a, b illustrate the composite median spatial distribution of SST (°C) during the past, and recent years. The climatological median SST values during 2005–2009 were in the range of 27–31 °C with values increasing from north to south BOB and west to east BOB. In comparison, the climatological median SST values during 2015–2019 were enhanced in the entire region except the northern regions of BOB. Interestingly, the spatial pattern in the decrease of SST in the study region is corresponding to the increase observed in the case of AOD, temperature, and CFO (Fig. 4c). Specifically, the SST decrease between the recent and past years is in the range of 0.2–0.4 °C over the NBOB region with mode values observed to be a greater (28.8 °C) during the past years as compared to the recent years (28.5 °C) over the NBOB region. Comparatively, the SST values has increased over the southern BOB region in the range of 0.2–0.8 °C between the recent years (median = 29.8 °C) and the past years (median = 29.4 °C). This is further substantiated by similar pattern in the trends of SST value over the region (Fig. 4d). The SST trends are decreasing in the NBOB with values of 0.02 °C year^{-1} and the same is increasing over the other grids in BOB at a rate of 0.02 °C year^{-1}. Note that the observed trends of robust decrease in SST in NBOB can be partially contributed by the combined effect of two effects: the enhanced aerosol direct radiative forcing and the aerosol-induced enhancement in cloud radiative forcing over the region (Supplementary Fig. 8).

DISCUSSION

In summary, the present study investigated the aerosol – cloud interactions using long-term multi-satellite observations during the pre-monsoon months. We find that aerosol loading is found to have increased by 27% between the recent decade and the past decade over the NBOB region. This can be attributed to prevalent westerly winds and regional transport of pollution which acts to accumulate anthropogenic aerosols over the NBOB region during the pre-monsoon season. Specifically, the aerosol loading over this outflow region is enhanced in an elevated layer between ~1 and 3 km, which is warming the atmospheric in the same layer. The warming leads to greater atmospheric stability in the lower troposphere. This can hinder vertical mixing and causes moisture trapping near the ocean surface[6,12,39], which explains the observed low-level moistening over NBOB. The radiative heating by the presence of elevated anthropogenic absorbing aerosol layers enhances the moisture convergence, and hence specific humidity (Supplementary Fig. 4) in the lower troposphere. Elevated aerosol-induced heating increases the buoyancy of the air above the cloud-topped marine boundary layer. The enhancement in buoyancy hinders entrainment of free troposphere dry air over the cloud top leading to maintaining the relative humidity of the boundary layer and consequently causing thicker clouds with

higher CWP[10]. This can explain our results that the low-level CFO is enhanced along with the increase of anthropogenic aerosol extinction at an elevated location (Supplementary Fig. 5). Satellite retrieved increasing trends of low-level cloud cover during the recent two decades over the outflow region of aerosol to the Northwest Indian Ocean, Atlantic Ocean, and north Pacific has been illustrated[42–49]. However, the influence of aerosol on cloud trends in those studies are not evident. As far as we know, only one previous observational study illustrates such strong aerosol-cloud trend association i.e., over the Southern China outflow region[50,51]. In that region, it was found that a decreasing trend of AOD of ~30% leads to an increase in liquid cloud cover by ~40% with winter season.

Nevertheless, low-level warm clouds are also highly sensitive to change in CDNC[52], and as these low-level clouds over NBOB are formed in a polluted boundary layer, aerosol-induced cloud microphysical processes cannot be ignored[19]. Previous studies like Jose et al.[20] and Khatri et al.[53] has shown the prevalence of anti-Twomey effect in smaller clouds (smaller liquid water path) over Northern India and BOB. Note that, the net observed effect of aerosols on low-level cloud occurrence trends over NBOB (in this study) could be the combined effect of the two opposite processes: aerosols induced anti-Twomey effect and elevated aerosol-induced semi-direct effect (Supplementary Fig. 5). Theoretically, the anti-Twomey effect over NBOB should result in a decreasing trend in low-level clouds over NBOB. In contrast, we observe a distinct positive trend in the low-level clouds, which indicates that SDE might be the dominant pathway affecting cloud trends in this region. Further, a distinct decrease in the middle, and high-level clouds in the recent years over the NBOB region is also observed (Supplementary Fig. 7) indicating a strong influence of semi-direct effect associated lower atmospheric stability on the cloud trends over this region.

Also, a perpetual challenge with empirical trend studies is absolute quantification of various process impact under a changing climate. For example, here, a skeptical argument could be that the observed aerosol-cloud-SST trend associations would be due to co-variability in meteorology under climate change. We discuss the following points in that context. First, modeling studies tend to show that the changing climate will lead to decreasing low-level cloud trends in marine conditions[6,39,54–56], and enhancement in trends of high cloud occurrences[21], which is opposite to our observations over NBOB. Second, similar to absorbing aerosols, GHG emissions can also induce lower tropospheric stability, but SDE-induced lower tropospheric stability has been found to be ~4 times stronger[57], and hence SDE would dominate the net effect compared to GHG-induced warming[6,12,58]. In agreement, many modeling studies have shown a semi-direct effect induced increasing low-level cloud cover in contrast to GHG's effects[10,39,54,58–60]. Lastly, the large-scale circulation over the NBOB region has not changed significantly from past years to the recent period (Supplementary Fig. 9). Nevertheless, the observed decadal changes and corroborating trends in aerosol, thermodynamics, and cloud cover are robust, suggesting potential physical cause-effect relationships. Taken together with the existing modeling work, our observational analysis is consistent towards concluding that SDE is an important process in governing the cloud trends in this region.

However, the detection of aerosol-cloud associations using satellite data alone has caveats. Residual or unnoticed clouds can contaminate the area of aerosol retrieval leading to an overestimation of aerosol optical depth and consequently affecting the association between aerosol and cloud properties[61]. Therefore, in this study, AOD samples greater than 1.0 were omitted to negate the impact of the cloud contamination of AOD retrievals, aerosol humidification, and meteorological co-variability on estimated quantitative trend magnitudes[3,62,63]. Nonetheless, our study underlines the significant impact of aerosols on potential sea – aerosol – atmosphere associations and advocates the need of coupled ocean-atmosphere-chemistry modeling for improved climate understanding over South Asia, which will eventually aid the efforts toward sustainable development goal on climate action.

METHODS

The Moderate Resolution Imaging Spectroradiometer (MODIS) instrument onboard the Aqua satellite is one of the main instruments used for examining the effect of aerosols on cloud cover. The uncertainty in the MODIS retrieved AOD is $\Delta AOD = \pm 0.03 \pm 0.05 AOD$ and $\Delta AOD = \pm 0.05 \pm 0.15 AOD$ over Ocean and land receptively[64,65]. The detailed MODIS/Aqua retrieval product algorithms are discussed in Remer et al.[64,65] and Platnick et al.[66]. Long-term MODIS/Aqua level-2 (Collection 6.1) data with a resolution of $0.1° \times 0.1°$ is used in the present study for the period of 2005–2019 during the pre-monsoon months of March through May.

Cloud-Aerosol Lidar and Infrared Pathfinder Satellite Observation (CALIPSO) level-3 (version 4–20) tropospheric aerosol profile data during all-sky conditions are used in this study for the examination of vertical profiles of the aerosol distribution. The extinction coefficient profile at 532 nm is used for the assessment of aerosol optical depth from Cloud-Aerosol Lidar with Orthogonal Polarization (CALIOP). The detailed algorithm for CALIOP aerosol retrievals and product information is described in the Garnier et al.[67].

The Atmospheric InfraRed Sounder (AIRS) instrument onboard the Aqua satellite gives vertical temperature and relative humidity (RH) profiles using the average kernel function algorithms[68]. The daily vertical temperature, and RH profiles at six different pressure levels (i.e., surface, 925, 850, 700, and 600hPa) are used in this study. MODIS/Aqua measures SST between 1 millimeter and 20 meters depth beneath the Ocean Surface using the 11-micron infrared channel. The details of MODIS/Aqua, CALIPSO, and AIRS datasets used in this study are provided in the supplementary table 1.

Aerosol and cloud data are co-located in time and space. Marine low-level clouds are constrained from MODIS/Aqua datasets during the pre-monsoon month using the several screening standards: (a) AOD (Aerosol Optical Depth) greater than 1.0 are excluded to avoid the cloud contamination, (b) CTP (Cloud Top Pressure) less than 680hPa are omitted to study the low-level clouds or shallow clouds only, and (c) Cloud Optical Depth (COD) greater than 23 are excluded to consider cumulus and stratocumulus clouds only.

MODIS/Aqua level-2 cloud product datasets are used to compute the cloud droplet number concentration (CDNC; cm^{-3}) using the equation suggested by Quaas et al.[69,70] and Brenguier et al.[71] as

$$CDNC = \alpha \tau_c^{\frac{1}{2}} r_e^{-\frac{5}{2}} \quad (1)$$

which is a combination of Eqs. (10) and (13) in Brenguier et al.[71], where $\alpha = 1.37 \times 10^{-5}\ m^{-0.5}$, and τ_c and r_e are the COD and cloud CER respectively. The sensitivity of clouds to aerosol perturbations is determined by cloud susceptibility. Cloud susceptibility infers how much a cloud is affected by perturbation in aerosol loading. To quantify the sensitivity of cloud fraction occurrences (CFO) to variations in aerosol loading, cloud susceptibility is computed using the equation recommended by Chen et al.[14] and Sorooshian et al.[72]. Cloud susceptibility (S) can be conveyed in terms of cloud occurrence frequency (CFO), and AOD as a proxy of CCN as

$$S = -\frac{\partial \ln(CFO)}{\partial \ln(AOD)} \quad (2)$$

DATA AVAILABILITY

The authors would be thankful to the members of the science team of MODIS, CALIPSO, and AIRS for providing, and maintaining different datasets used in the study. MODIS/Aqua is accessible online from Atmosphere Archive & Distribution

System Distributed Active Archive Center (https://ladsweb.modaps.eosdis.nasa.gov/). CALIPSO, AIRS, and TRMM datasets are accessible from GES DISC (Data archive and information services for Atmospheric Composition, Water & Energy Cycles, Climate Variability; https://daac.gsfc.nasa.gov/).

CODE AVAILABILITY

The codes used for the analysis in this study are available upon request from the corresponding author.

Received: 13 December 2022; Accepted: 2 August 2023;
Published online: 06 September 2023

REFERENCES

1. Seinfeld, J. H. et al. Improving our fundamental understanding of the role of aerosol- cloud interactions in the climate system. *Proc. Natl Acad. Sci. USA* **113**, 5781–5790 (2016).
2. Kant, S., Panda, J., Pani, S. K. & Wang, P. K. Long-term study of aerosol–cloud–precipitation interaction over the eastern part of India using satellite observations during pre-monsoon season. *Theor. Appl. Climatol.* **136**, 605–626 (2019).
3. Kant, S., Panda, J. & Gautam, R. A seasonal analysis of aerosol-cloud-radiation interaction over Indian region during 2000–2017. *Atmos. Environ.* **201**, 212–222 (2019).
4. Sarangi, C., Kanawade, V. P., Tripathi, S. N., Thomas, A. & Ganguly, D. Aerosol-induced intensification of cooling effect of clouds during Indian summer monsoon. *Nat. Commun.* **9**, 3754 (2018).
5. Ackerman, A. S. et al. Effects of aerosols on cloud albedo: evaluation of twomey's parameterization of cloud susceptibility using measurements of ship tracks. *J. Atmos. Sci.* **57**, 2684–2695 (2000).
6. Allen, R. J. et al. Observationally constrained aerosol–cloud semi-direct effects. *npj Clim. Atmos. Sci.* **2**, 16 (2019).
7. Hansen, J., Sato, M., Lacis, A. & Ruedy, R. The missing climate forcing. *Philos. Trans. R. Soc. Lond. Ser. B: Biol. Sci.* **352**, 231–240 (1997).
8. Kaufman, Y. J. & Koren, I. Smoke and pollution aerosol effect on cloud cover. *Science* **313**, 655–658 (2006).
9. Wilcox, E. Stratocumulus cloud thickening beneath layers of absorbing smoke aerosol. *Atmos. Chem. Phys.* **10**, 11769–11777 (2010).
10. Johnson, B., Shine, K. & Forster, P. The semi-direct aerosol effect: Impact of absorbing aerosols on marine stratocumulus. *Q. J. R. Meteorol. Soc.* **130**, 1407–1422 (2004).
11. Wilcox, E. Direct and semi-direct radiative forcing of smoke aerosols over clouds. *Atmos. Chem. Phys.* **12**, 139–149 (2012).
12. Wilcox, E. M. et al. Black carbon solar absorption suppresses turbulence in the atmospheric boundary layer. *Proc. Natl Acad. Sci. USA* **113**, 11794–11799 (2016).
13. Stjern, C. W. et al. Rapid adjustments cause weak surface temperature response to increased black carbon concentrations. *J. Geophys. Res. Atmospheres* **122**, 11–462 (2017).
14. Chen, Y.-C., Christensen, M. W., Stephens, G. L. & Seinfeld, J. H. Satellite-based estimate of global aerosol–cloud radiative forcing by marine warm clouds. *Nat. Geosci.* **7**, 643–646 (2014).
15. Koch, D. & Del Genio, A. D. Black carbon semi-direct effects on cloud cover: review and synthesis. *Atmos. Chem. Phys.* **10**, 7685–7696 (2010).
16. Sand, M. et al. A standardized global climate model study showing unique properties for the climate response to black carbon aerosols. *J. Clim.* **28**, 2512–2526 (2015).
17. Hodnebrog, Ø., Myhre, G. & Samset, B. H. How shorter black carbon lifetime alters its climate effect. *Nat. Commun.* **5**, 5065 (2014).
18. Norris, J. R. Has northern Indian ocean cloud cover changed due to increasing anthropogenic aerosol? *Geophys. Res. Lett.* **28**, 3271–3274 (2001).
19. Bony, S., Collins, W. D. & Fillmore, D. W. Indian Ocean low clouds during the winter monsoon. *J. Clim.* **13**, 2028–2043 (2000).
20. Jose, S., Nair, V. S. & Babu, S. S. Anthropogenic emissions from south Asia reverses the aerosol indirect effect over the northern Indian ocean. *Sci. Rep.* **10**, 18360 (2020).
21. Ceppi, P., Brient, F., Zelinka, M. D. & Hartmann, D. L. Cloud feedback mechanisms and their representation in global climate models. *Wiley Interdiscip. Rev. Clim. Chang.* **8**, e465 (2017).
22. Leibensperger, E. M. et al. Climatic effects of 1950–2050 changes in us anthropogenic aerosols–part 1: aerosol trends and radiative forcing. *Atmos. Chem. Phys.* **12**, 3333–3348 (2012).
23. Thomas, A., Kanawade, V. P., Sarangi, C. & Srivastava, A. K. Effect of covid-19 shutdown on aerosol direct radiative forcing over the Indo-Gangetic plain outflow region of the Bay of Bengal. *Sci. Total. Environ.* **782**, 146918 (2021).
24. Srivastava, A., Misra, A., Kanawade, V. P. & Devara, P. Aerosol characteristics in the utls region: a satellite-based study over north India. *Atmos. Environ.* **125**, 222–230 (2016).
25. Sarin, T., Vinoj, V., Swain, D., Landu, K. & Suhas, E. Aerosol induced changes in sea surface temperature over the Bay of Bengal due to covid-19 lockdown. *Front. Mar. Sci.* **8**, 648566 (2021).
26. Lakshmi, N., Nair, V. S. & Suresh Babu, S. Vertical structure of aerosols and mineral dust over the Bay of Bengal from multisatellite observations. *J. Geophys. Res. Atmos.* **122**, 12–845 (2017).
27. Nair, V. S., Babu, S. S., Manoj, M., Moorthy, K. K. & Chin, M. Direct radiative effects of aerosols over south Asia from observations and modeling. *Clim. Dyn.* **49**, 1411–1428 (2017).
28. Nair, V. S. et al. Black carbon aerosols over the Himalayas: direct and surface albedo forcing. *Tellus B: Chem. Phys. Meteorol.* **65**, 19738 (2013).
29. Corrigan, C., Roberts, G., Ramana, M., Kim, D. & Ramanathan, V. Capturing vertical profiles of aerosols and black carbon over the Indian ocean using autonomous unmanned aerial vehicles. *Atmos. Chem. Phys.* **8**, 737–747 (2008).
30. Fadnavis, S. et al. Elevated aerosol layer over south Asia worsens the Indian droughts. *Sci. Rep.* **9**, 10268 (2019).
31. Moorthy, K. K., Satheesh, S. & Kotamarthi, V. Evolution of aerosol research in India and the rawex-gvax: an overview. *Curr. Sci.* **111**, 53–75 (2016).
32. Sarangi, C., Tripathi, S., Mishra, A., Goel, A. & Welton, E. Elevated aerosol layers and their radiative impact over Kanpur during monsoon onset period. *J. Geophys. Res. Atmos.* **121**, 7936–7957 (2016).
33. Prakash, J. et al. Characterization, sources, and atmospheric transformation of a few key short-lived climate pollutants (SLCPs) at a rural super-site in the Indo-Gangetic Plain (IGP) of India. *Environ. sci. Atmos.* **2**, 517–538 (2022).
34. Nair, P. R., George, S. K., Aryasree, S. & Jacob, S. Chemical composition of aerosols over Bay of Bengal during pre-monsoon: Dominance of anthropogenic sources. *J. Atmos. Sol.-Terrestrial Phys.* **109**, 54–65 (2014).
35. Reddy, L. A. K. et al. Chemical characteristics of PM 10 aerosols and airmass trajectories over Bay of Bengal and Arabian Sea during ICARB. *J. Earth Syst. Sci.* **117**, 345–352 (2008).
36. Mhawish, A. et al. Aerosol characteristics from earth observation systems: a comprehensive investigation over south Asia (2000–2019). *Remote. Sens. Environ.* **259**, 112410 (2021).
37. Thomas, A., Sarangi, C. & Kanawade, V. P. Recent increase in winter hazy days over Central India and the Arabian Sea. *Sci. Rep.* **9**, 1–10 (2019).
38. Zhang, J., Zhou, X., Goren, T. & Feingold, G. Albedo susceptibility of northeastern pacific stratocumulus: the role of covarying meteorological conditions. *Atmos. Chem. Phys.* **22**, 861–880 (2022).
39. Allen, R. & Sherwood, S. Aerosol-cloud semi-direct effect and land-sea temperature contrast in a GCM. *Geophys. Res. Lett* **37**, L07702 (2010).
40. Lee, S. S., Penner, J. E. & Saleeby, S. M. Aerosol effects on liquid-water path of thin stratocumulus clouds. *J. Geophys. Res. Atmospheres* **114**, D07204 (2009).
41. Jia, H., Ma, X., Yu, F., Liu, Y. & Yin, Y. Distinct impacts of increased aerosols on cloud droplet number concentration of stratus/stratocumulus and cumulus. *Geophys. Res. Lett.* **46**, 13517–13525 (2019).
42. Norris, J. R. et al. Evidence for climate change in the satellite cloud record. *Nature* **536**, 72–75 (2016).
43. Geiss, A. & Marchand, R. Cloud responses to climate variability over the extratropical oceans as observed by MISR and MODIS. *Atmos. Chem. Phys.* **19**, 7547–7565 (2019).
44. Cherian, R. & Quaas, J. Trends in AOD, clouds, and cloud radiative effects in satellite data and CMIP5 and CMIP6 model simulations over aerosol source regions. *Geophys. Res. Lett.* **47**, e2020GL087132 (2020).
45. Dey, S., Nishant, N., Sengupta, K. & Ghosh, S. Cloud climatology over the oceanic regions adjacent to the Indian subcontinent: inter-comparison between passive and active sensors. *Int. J. Remote. Sens.* **36**, 899–916 (2015).
46. Prabhu, A. & Pandithurai, G. Isccp observed large-scale cloud features over the indo-pacific, southern annular mode and Indian summer monsoon. *Polar Sci.* **18**, 167–175 (2018).
47. Rao, S. & Dey, S. Consistent signal of aerosol indirect and semi-direct effect on water clouds in the oceanic regions adjacent to the Indian subcontinent. *Atmos. Res.* **232**, 104677 (2020).
48. Kumar, H. & Tiwari, S. Climatology, trend of aerosol-cloud parameters and their correlation over the northern Indian ocean. *Geosci. Front.* **14**, 101563 (2023).
49. Sharma, P., Ganguly, D., Sharma, A. K., Kant, S. & Mishra, S. Assessing the aerosols, clouds and their relationship over the northern bay of bengal using a global climate model. *Earth Space Sci.* **10**, e2022EA002706 (2023).
50. Benas, N., Meirink, J. F., Karlsson, K.-G., Stengel, M. & Stammes, P. Satellite observations of aerosols and clouds over southern china from 2006 to 2015:

analysis of changes and possible interaction mechanisms. *Atmos. Chem. Phys.* **20**, 457–474 (2020).
51. Bretherton, C. S., Blossey, P. N. & Jones, C. R. Mechanisms of marine low cloud sensitivity to idealized climate perturbations: A single-les exploration extending the cgils cases. *J. Adv. Model. Earth Syst.* **5**, 316–337 (2013).
52. Schwartz, S. & Slingo, A. *Enhanced Shortwave Cloud Radiative Forcing Due To Anthropogenic Aerosols* (Springer, 1996).
53. Khatri, P. et al. Increased aerosols can reverse twomey effect in water clouds through radiative pathway. *Sci. Rep.* **12**, 20666 (2022).
54. Perlwitz, J. & Miller, R. L. Cloud cover increase with increasing aerosol absorptivity: a counterexample to the conventional semidirect aerosol effect. *J. Geophys. Res. Atmospheres* **115**, D08203 (2010).
55. Liu, H., Koren, I., Altaratz, O. & Chekroun, M. D. Opposing trends of cloud coverage over land and ocean under global warming. *Atmos. Chem. Phys. Discuss.* **23**, 6559–6569 (2023).
56. Prijith, S., Lima, C., Ramana, M. & Sai, M. S. Intra-seasonal contrasting trends in clouds due to warming induced circulation changes. *Sci. Rep.* **11**, 16985 (2021).
57. Ramanathan, V. et al. Atmospheric brown clouds: impacts on south Asian climate and hydrological cycle. *Proc. Natl Acad. Sci. USA* **102**, 5326–5333 (2005).
58. Allen, R. J. et al. Surface warming and wetting due to methane's long-wave radiative effects muted by short-wave absorption. *Nat. Geosci.* **16**, 314–320 (2023).
59. Wang, C. A modeling study on the climate impacts of black carbon aerosols. *J. Geophys. Res. Atmospheres* **109**, D03106 (2004).
60. Roeckner, E. et al. Impact of carbonaceous aerosol emissions on regional climate change. *Clim. Dyn.* **27**, 553–571 (2006).
61. Sogacheva, L. et al. Spatial and seasonal variations of aerosols over China from two decades of multi-satellite observations–part 1: ATSR (1995–2011) and MOODIS c6. 1 (2000–2017). *Atmos. Chem. Phys.* **18**, 11389–11407 (2018).
62. Kant, S., Panda, J. & Manoj, M. A satellite observation-based analysis of aerosol-cloud-precipitation interaction during the February 2016 unseasonal heatwave episode over Indian region. *Aerosol Air Qual. Res.* **19**, 1508–1525 (2019).
63. Kant, S., Panda, J., Rao, P., Sarangi, C. & Ghude, S. D. Study of aerosol-cloud-precipitation-meteorology interaction during a distinct weather event over the Indian region using wrf-chem. *Atmos. Res.* **247**, 105144 (2021).
64. Remer, L. A. et al. The MODIS aerosol algorithm, products, and validation. *J. Atmos. Sci.* **62**, 947–973 (2005).
65. Remer, L. A. et al. Global aerosol climatology from the MODIS satellite sensors. *J. Geophys. Res. Atmos.* **113**, D14S07 (2008).
66. Platnick, S. et al. The MODIS cloud optical and microphysical products: collection 6 updates and examples from terra and aqua. *IEEE Trans. Geosci. Remote Sens.* **55**, 502–525 (2016).
67. Garnier, A. et al. Version 4 CALIPSO imaging infrared radiometer ice and liquid water cloud microphysical properties–part II: Results over oceans. *Atmos. Meas. Tech.* **14**, 3277–3299 (2021).
68. Maddy, E., Barnet, C., Goldberg, M., Sweeney, C. & Liu, X. Co2 retrievals from the atmospheric infrared sounder: Methodology and validation. *J. Geophys. Res. Atmospheres* **113**, D11301 (2008).
69. Quaas, J., Boucher, O. & Lohmann, U. Constraining the total aerosol indirect effect in the lmdz and ECHAM4 GCMs using MODIS satellite data. *Atmos. Chem. Phys.* **6**, 947–955 (2006).
70. Quaas, J., Stevens, B., Stier, P. & Lohmann, U. Interpreting the cloud cover – aerosol optical depth relationship found in satellite data using a general circulation model. *Atmos. Chem. Phys.* **10**, 6129–6135 (2010).
71. Brenguier, J. et al. An overview of the ace-2 cloudy column closure experiment. *Tellus B* **52**, 815–827 (2000).
72. Sorooshian, A., Feingold, G., Lebsock, M. D., Jiang, H. & Stephens, G. L. On the precipitation susceptibility of clouds to aerosol perturbations. *Geophys. Res. Lett.* **36**, L13803 (2009).

ACKNOWLEDGEMENTS

C.S. acknowledges support from the New Faculty Initiation Grant of IIT Madras. C.S. and S.K. acknowledges support from the Science and Engineering Research Board, Department of Science and Technology, Government of India under the "Start-up Research Grant (SRG) scheme" (Grant SRG/2020/001658). E.M.W. is supported by NASA Grant # 80NSSC18K0846.

AUTHOR CONTRIBUTIONS

S.K.: methodology, investigation, visualization, writing the initial draft, reviewing and editing the manuscript. C.S.: conceptualization, methodology, supervision, writing the manuscript, reviewing and editing the manuscript., funding acquisition. E.W.: reviewing and editing the manuscript.

COMPETING INTERESTS

The authors declare no competing interests.

ADDITIONAL INFORMATION

Supplementary information The online version contains supplementary material available at https://doi.org/10.1038/s41612-023-00443-x.

Correspondence and requests for materials should be addressed to Chandan Sarangi.

Reprints and permission information is available at http://www.nature.com/reprints

Publisher's note Springer Nature remains neutral with regard to jurisdictional claims in published maps and institutional affiliations.